Super-Resolution Imaging of Amyloid Structures over Extended Times Using Transient Binding of Single Thioflavin T Molecules

Kevin Spehar[+][a], Tianben Ding[+][b], Yuanzi Sun[a,c], Niraja Kedia[a], Jin Lu[b], George R. Nahass[a], Matthew D. Lew*[b], and Jan Bieschke*[a,d]

Abstract: Oligomeric amyloid structures are crucial therapeutic targets in Alzheimer's and other amyloid diseases. However, these oligomers are too small to be resolved by standard light microscopy. We have developed a simple and versatile tool to image amyloid structures using Thioflavin T without the need for covalent labeling or immunostaining. Dynamic binding of single dye molecules generates photon bursts that are used for fluorophore localization on a nanometer scale. Thus, photobleaching cannot degrade image quality, allowing for extended observation times. Super-resolution Transient Amyloid Binding (TAB) microscopy promises to directly image native amyloid using standard probes and record amyloid dynamics over minutes to days. We imaged amyloid fibrils from multiple polypeptides, oligomeric, and fibrillar structures formed during different stages of amyloid-β aggregation, as well as the structural remodeling of amyloid-β fibrils by the compound epi-gallocatechin gallate (EGCG).

Amyloid diseases, such as Alzheimer's disease (AD) and Type II diabetes are the most prevalent, yet incurable, aging-related diseases. Protein misfolding and amyloid formation underlie their disease progression.[1] The 42 amino-acid residue amyloid-beta peptide (Aβ42) is the main component of extracellular plaques in the brains of AD patients.[2,3] Nanometer-sized aggregation intermediates are the main culprits in amyloid toxicity.[4,5] A quantitative understanding of their dynamics requires new tools that can visualize these structures, which are too small to be resolved by conventional light microscopy.

Single-molecule (SM) super-resolution (SR) fluorescence microscopy techniques, such as (f)PALM,[6,7] (d)STORM,[8,9] and others, overcome the resolution barrier posed by optical diffraction (~250 nm for visible light) and allow us to visualize structures with nanoscale resolution in living cells. Utilizing a variety of mechanisms,[10,11] most techniques rely upon switching these molecules between bright and dark states to reduce the effective concentration of fluorescing molecules within a sample. A related SM-SR technique, called PAINT,[12] uses combinations of fluorophore binding and unbinding, diffusion into and out of the imaging plane, and/or spectral shifts upon binding to generate flashes of SM fluorescence. In these SR techniques, many blinking events are recorded over time, and image-processing algorithms[13] measure the position of each bright molecule with high precision. A SR image is reconstructed in a "pointillist" fashion from the locations of these single fluorophores.[14–16]

SR microscopy commonly leverages tagging techniques that involve covalent attachment[9,17–19] or intrinsical intercalation[20] of a fluorophore to the biomolecule of interest. To produce high-resolution images, biological targets must be densely labeled with fluorescent molecules,[21,22] which can potentially alter the structure of interest. Furthermore, photobleaching of tagged fluorescent molecules limits measurement time and prevents long-term imaging of targets. Recently, following the development of PAINT, binding-activated or transiently-binding probes have expanded the scope of SR imaging to functional studies.[23–25] When in the immediate vicinity of their target, these probes either become fluorescent, temporarily bind to the target, or both, thereby creating a "flash" of fluorescence that is used to locate the target of interest. Amyloidophilic dyes such as Thioflavin T (ThT), Thioflavin S, and Congo red specifically bind to structural motifs of amyloid.[26,27] Their absorbance and fluorescence have been used for close to 100 years in the histological staining of amyloid structures and in resolving aggregation kinetics *in vitro*.[27–29]

Here, we report a technique to image amyloid structures on the nanometer scale, called Transient Amyloid Binding (TAB) imaging. TAB imaging uses standard amyloid dyes such as Thioflavin T, without the need for covalent modification of the amyloid protein or immunostaining. Our technique mates SR microscopy with histological staining techniques and is compatible with epi-fluorescence and total internal reflection fluorescence (TIRF) microscopy. We therefore envision that it will allow a much wider application of SR imaging to the diagnosis and cellular study of amyloid diseases than was previously possible.

The fluorescence of ThT increases upon binding to amyloid proteins, transforming dark ThT in solution into its bright state.[26,30] The molecules emit fluorescence until they photobleach or dissociate from the structure. These transient binding dynamics enabled us to record movies of 'blinking' ThT molecules, localize their positions with high precision, and reconstruct the underlying amyloid structure. To demonstrate the concept of TAB imaging, we imaged Aβ42 fibrils adsorbed to an imaging chamber using an epi-fluorescence microscope with a highly-inclined 488-nm excitation laser (Figs. 1A and S1A, and Table S1). An imaging buffer containing 1 - 2.5 μM ThT, was pipetted into the chamber (Supporting Note 11, and Table S2),

[a] K. Spehar[+], Y. Sun, Dr. N. Kedia, G. R. Nahass, Prof. J. Bieschke*
Department of Biomedical Engineering
Washington University in St. Louis
St. Louis, MO 63130 (USA)
E-mail: bieschke@wustl.edu
[b] T. Ding[+], Dr. J. Lu, Prof. M. D. Lew*
Department of Electrical and Systems Engineering
Washington University in St. Louis
St. Louis, MO 63130 (USA)
E-mail: mdlew@wustl.edu
[c] Y. Sun
Department of Energy, Environmental, and Chemical Engineering
Washington University in St. Louis
St. Louis, MO 63130 (USA)
[d] Prof. J. Bieschke*
MRC Prion Unit
UCL Institute of Prion Diseases
London, (UK)
E-mail: j.bieschke@ucl.ac.uk
[+] These authors contributed equally to this work.

Supporting information for this article is given via a link at the end of the document.

and 5,000-10,000 imaging frames were recorded with 20 ms camera exposure. The image sequence (Fig. 1B) and temporal trace of photons detected (Fig. 1C) demonstrate the blinking of single ThT molecules. We found that each blinking event on average lasted 12 ms (Supporting Note 16, Fig. S2). A SR image with 20×20 nm^2 bin size (Fig. 1D) was reconstructed from multiple blinking events using ThunderSTORM[31] and a custom post-processing algorithm (Supporting Notes 13-15). The measured full-width at half-maximum (FWHM) of the reconstructed Aβ42 fibril over the length of the fibril is 60 ± 10 nm (Fig. 1E). Typical amyloid fibrils have diameters of 8-12 nm[32]. The measured width of the fibril likely arises from our localization precision[33] of 17 nm (FWHM: 40 nm), corresponding to a median of 296 photons detected per ThT localization (Table S3).

The blinking characteristics of ThT are determined by the binding and photobleaching kinetics of the dye. Binding affinity and specificity may be affected by hydrophobic interactions[34]. Therefore, we varied the NaCl concentration and pH as well as ThT concentration of the buffer to test their influence on ThT blinking (Supporting Note 17, Fig. S3). We found that the NaCl concentrations (10 - 500 mM) and pH of the imaging buffer (6.0 - 8.6) had little effect on the blinking of ThT on Aβ42 fibrils. However, high NaCl concentration (500 mM) and low pH (6.0) lowered the fluorescence background of unbound ThT. This corresponds to fewer bursts that occurred off of the amyloid fibril, thus improving TAB imaging performance. On the other hand, we also found that the blinking rate of ThT, and thus the rate of localizations per time, is approximately proportional to ThT concentration. In this paper, the ThT concentration was chosen to maximize the localization rate of ThT binding events while avoiding too much fluorescence background. These results demonstrate that TAB imaging of amyloid structures is amenable to a wide variety of buffer conditions. Unlike other SR methods that employ photoswitching of organic dyes,[9] TAB does not require the addition of specific reducing agents or oxygen scavengers[18] to the buffer.

We verified that TAB SR imaging faithfully reproduces the structure of Aβ fibrils by comparing TAB images to those of conventional fluorescent tags. First, Aβ42 fibrils were intrinsically labeled with Alexa-647 and imaged using conventional epi-fluorescence microscopy. Their morphology matched the TAB SR image of the same fibril (Figs. 2A-C). Next, we directly compared SR TAB images to dSTORM imaging. Aβ42 fibrils were tagged using monoclonal anti-Aβ antibody 6E10 and Alexa-647 labeled goat-anti-mouse secondary antibody, and imaged by dSTORM of the Alexa-647 dye, followed by TAB imaging of the ThT dye. Typical dSTORM imaging using Alexa-647 gives localization precision of 6 nm (FWHM: 14 nm) that corresponds to 3,700 photons detected per localization (Fig. S4 and Table S3). Both dSTORM and TAB imaging reveal a thin and uniform fibril structure (Figs. 2D-G). Reconstructed images from SR TAB microscopy gave comparable or better resolution than the conventional label-based SR technique. The measured FWHM of the reconstructed Aβ42 fibril using Alexa-647 was 80 ± 30 nm (Fig. 2D), while the TAB reconstruction on the same fibril yielded a FWHM of 60 ± 10 nm (Fig. 2F). This resolution is comparable to reported apparent fibril widths of 40-50 nm *via* dSTORM imaging using covalently modified Aβ.[18] A resolution of 14 nm was reported for synuclein fibrils that were imaged *via* binding activated fluorescence using a conjugated oligothiophene p-FTAA.[23] However, this resolution was achieved at the expense of limited observation times. Our results also demonstrate that the TAB technique relaxes the challenges stemming from the high labeling density and uniformity requirements[22] of conventional SR methods.

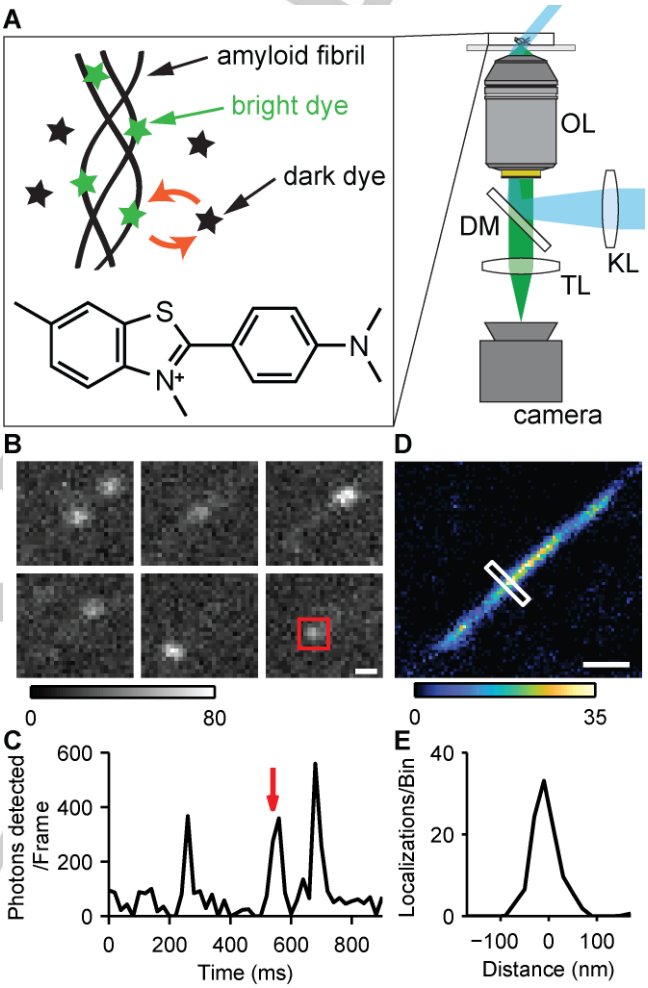

Figure 1. TAB microscopy. (A) Pseudo-TIRF illumination (cyan) excites fluorophores within the sample, and collected fluorescence (green) is imaged onto a camera. KL, widefield lens; OL, objective lens; DM, dichroic mirror; TL, tube lens. Two epi-fluorescence microscopes (1 and 2) were used for image acquisition (Fig. S1, Table S1). Inset: transient binding, fluorescence activation, and unbinding of ThT and its chemical structure. (B) ThT blinking on an Aβ42 fibril. Scale bar: 300 nm. Grey scale: photons/pixel. (C) Integrated photons detected over time within the red square in B. The red arrow indicates the frame containing the square in B. (D) TAB SR image of the Aβ42 fibril. Scale bar: 300 nm. Color scale: localizations/bin. (E) Cross-section of the white box across the fibril in D.

We next explored the versatility of ThT as a probe for TAB imaging of various amyloid structures (Fig. S5). We prepared fibrils of Aβ40, α-synuclein, islet amyloid polypeptide (IAPP), tau protein and light chain (AL) amyloid, adsorbed them to glass surfaces, and imaged them. We were able to reconstruct images with apparent fibril widths of 40 – 80 nm for all polypeptides, which demonstrates that ThT can be used for SR imaging across a wide variety of targets. Some amyloids produced

reconstructions with wider apparent fibril widths than others, which may reflect differences in the binding affinities and the quantum yields of ThT on different fibrillar structures.[26,35] The synthesis and characterization of new dyes with different affinities may improve TAB image quality on such amyloids in the future.

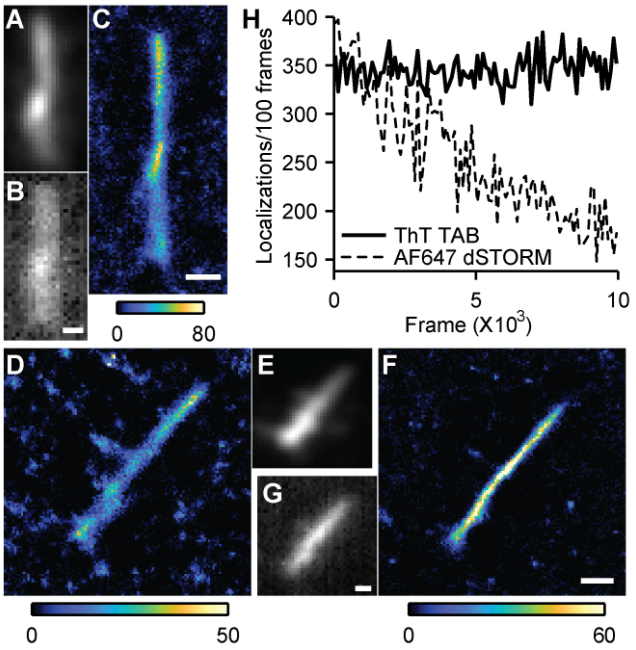

Figure 2. TAB SR imaging compared to conventional labelling. (A) Diffraction-limited image of an intrinsically-labeled Aβ42 fibril (4.2 % Aβ42-Alexa 647). (B) Diffraction-limited ThT image of the fibril in A. (C) TAB SR image of the fibril in A. (D) Conventional SR image of an Aβ42 fibril using Alexa-647 antibody staining. (E) Diffraction-limited image of D using Alexa-647. (F) TAB SR image of D. (G) Diffraction-limited ThT image of D. Color bars: localizations/bin. Scale bars: 300 nm. (H) Localizations per 100 frames over time for TAB and dSTORM imaging.

Thioflavin T is well-known to bind to mature amyloid fibrils. However, it would be valuable to also image intermediates of the aggregation pathway. We therefore explored whether TAB imaging could visualize different stages of the amyloid aggregation process. We generated Aβ40 aggregates from the late lag phase (t_1, 8 h), the growth phase (t_2, 24 h), and the late plateau phase (t_3, 66 h) of ThT kinetics (Fig. 3A) and verified aggregate morphologies by atomic force microscopy (AFM, Fig. 3B). Aggregates from t_1 corresponded to spherical oligomers, t_2 to single fibrils, and t_3 to fibril clusters, respectively.

We performed TAB imaging of the Aβ40 aggregates in a pseudo-TIRF microscope (Fig. S1B). Strikingly, TAB imaging was able to reconstruct spherical Aβ40 structures from an early stage of aggregation (Fig. 3D). These structures were measured to have dimensions of 4 - 5 nm by AFM, and therefore constitute typical Aβ40 oligomers.[36] Being able to accurately image oligomeric structures is important to capture the dynamics of Aβ aggregation and may open the door for future applications in cellular imaging of oligomeric structures.

To image the dynamics of amyloid formation, it is essential to have a robust tool that can follow the structure of a single aggregate over hours or more. We analyzed the stability of TAB imaging over time in three ways. First, we tested whether the localization rate remained constant within a single imaging experiment. We counted localization events in blocks of 100 frames across fibrils of various sizes and observed that the number of localizations did not change during the acquisition of an image stack (typically 1.5-3.5 min., Fig. 2H, Fig. S6A). In contrast, the localization rate of Alexa-647 in dSTORM dropped

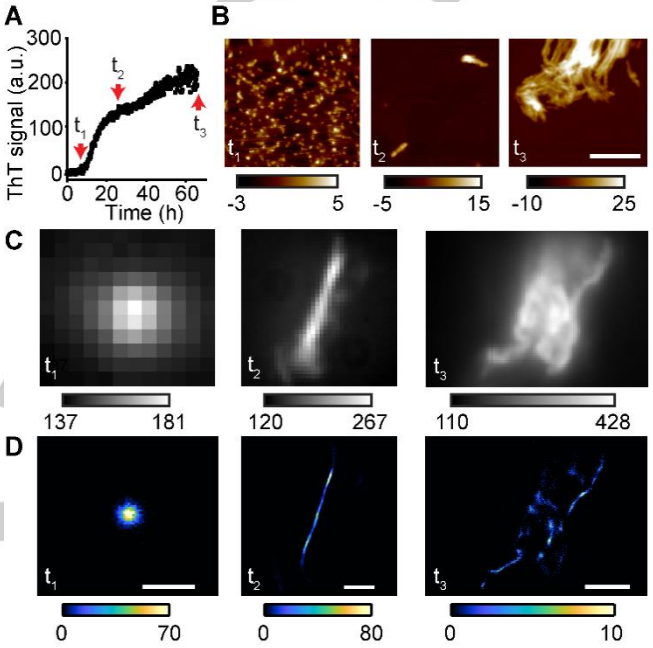

to less than half in a similar time frame.

Figure 3. Visualization of Aβ40 structures at various aggregation stages. (A) Aggregation kinetics of Aβ40 measured by ThT fluorescence. t1 (8 h), t2 (24 h), and t3 (66 h) represent oligomers, early fibrils and late fibril clusters, respectively. (B) AFM images of Aβ40 at t1, t2, and t3. Color bar in nm. Scale bars: 350 nm. (C) Diffraction-limited images of Aβ40 aggregates using ThT fluorescence at t1, t2, and t3. (D) TAB SR images of the structures in C. Fluorescence from out-of-focus structures decreased localizations in t3. Scale bars for t1, t2, and t3 are 0.5, 1, and 2.5 µm, respectively.

Further, we tested whether the localization rate remained constant over extended observation times. We imaged an Aβ42 fibril 17 times over 24 h, and counted localization events in blocks of 100 frames for each acquisition. We observed that the TAB reconstructions and the number of localizations remained approximately constant over the 24-hour acquisition (Fig. S6B and C). Therefore, TAB imaging with ThT is robust to photobleaching and capable of producing multiple time-lapse SR images, which can involve the localization of over 100,000 ThT molecules on a single fibril.

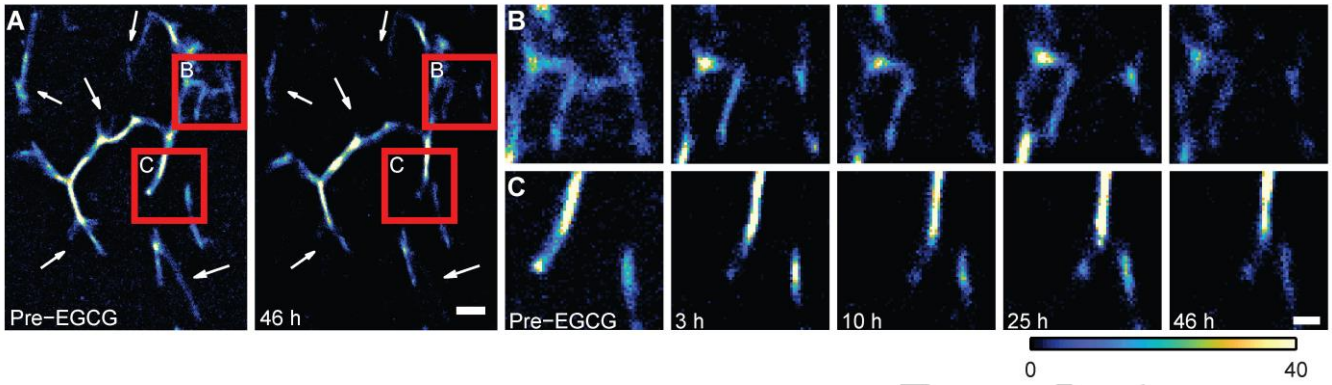

Figure 4. TAB SR images of Aβ42 fibril remodeling. (A) Aβ42 before and after a 46-hour reaction with EGCG (1 mM). White arrows denote regions with distinct changes. Scale bar: 500 nm. (B and C) Time-lapse TAB images of regions denoted by red squares in A, recorded before and 3, 10, 25, and 46 h after adding EGCG; scale bar: 200 nm; color bar denotes localizations/bin.

We next validated the capability of TAB for SR imaging over the course of hours to days. The time-lapse images (Figs. 4 and S7, and Movie S1) show the dissolution and remodeling of Aβ42 fibrils by epi-gallocatechin gallate (EGCG). Remarkably, TAB imaging captured the structural dynamics of amyloid fibrils for ~2 days, allowing us to observe remodeling over tens of micrometers with ~16 nm precision. In this experiment, we observed dynamics that were slower than at 37°C in solution,[36] most likely due to the lack of agitation of fibrils that were adsorbed to the glass surface and to incubation at room temperature.

The success of these experiments demonstrates the capability of TAB imaging to follow the dynamics of amyloid structures with nanometer resolution and ~minute temporal resolution over extended periods. This capability will be essential for visualizing drugs acting on amyloid structures to gain insight into their molecular-scale interactions with amyloid structures.

Previous studies have imaged ThT binding to dried amyloid samples through photoactivation (dSTORM).[20] We report SR imaging of a wide variety of fibrils and aggregation intermediates using transient binding of one of the most widely used amyloid dyes, Thioflavin T, which allows for extended observation times compared to dSTORM and similar techniques. While the use of binding dynamics of novel amyloid dye molecules may increase photon yield,[38] the ubiquity and versatility of ThT in amyloid staining should facilitate its adoption in nanoscopic imaging. We therefore expect that the use of TAB imaging can be expanded easily to a variety of substrates and conditions.

A critical challenge in preparing samples for SR microscopy is the need for high labeling density and uniformity, necessitating a large number of covalent modifications of, or antibodies attached to, the biomolecule of interest. Transient binding strategies, like PAINT and TAB imaging, reduce the complexity of sample preparation but potentially at the cost of requiring specific buffer conditions for efficient single-molecule blinking. Further, some transient labeling strategies, whose fluorophores emit fluorescence regardless of their binding state, require TIRF illumination to reduce background fluorescence for single-molecule imaging. Our results demonstrate that TAB SR microscopy maintains the simplicity of transient labeling methods while remaining robust to a wide variety of imaging conditions. ThT blinking is readily detectable across a range of pH and salt concentrations. TAB SR imaging performs well with both widefield epi-fluorescence and TIRF illumination strategies, because ThT becomes much brighter when bound to amyloid than in its unbound state. This flexibility and robustness allow TAB imaging to work in tandem with other dyes or molecules that probe specific proteins or biomolecules. TAB SR microscopy is also adept at continuous imaging for long periods of time without image degradation due to photobleaching, a major advantage over conventional SR techniques.

In contrast, photobleaching of dyes limits observation times in conventional SR techniques.[9] Previous studies using binding-activated probe molecules also had limited observation times, since the probe molecules bound irreversibly to the amyloid fibril.[23] Since TAB generates blinking by transient ThT binding, it is inherently robust to photobleaching. It should be noted that fluorescence background increased in the presence of EGCG. This increase is most likely because EGCG, a potent antioxidant, reduces photobleaching of ThT like other antioxidants, such as ascorbic acid, increases the number of photons per blinking event in other SR imaging.[37]

In summary, TAB SR microscopy is a flexible imaging technique that can provide images of amyloid structures with nanometer resolution over observation times of hours. It is capable of imaging various stages of amyloid aggregation as well as dynamic imaging of fibrillar remodeling by an anti-amyloid drug. Nanoscale imaging of aggregation intermediates will provide a clearer understanding of which structures are toxic to cells and will pave the road for further study into molecular mechanisms of AD and other amyloid diseases.

Experimental Section

All experimental details can be found in the accompanying supporting information.

Acknowledgements

Research reported in this publication was supported by the National Science Foundation under grant number ECCS-1653777 and by the National Institute of General Medical

Sciences of the National Institutes of Health under grant number R35GM124858 to MDL, and the Hope Center for Neurological Disorders pilot grant to JB. The authors would like to thank E. Illes-Toth and K. Andrich for protein preparation; B. Holmes and M. Diamond (UT Southwest) for the gift of tau protein, U. Hegenbart and S. Schönland (Amyloidosezentrum Heidelberg) for providing LC samples, and O. Zhang for technical assistance.

Keywords: amyloid beta-peptides • long-term imaging • single-molecule localization microscopy • single-molecule studies

[1] J. D. Harper, P. T. Lansbury, *Annu. Rev. Biochem.* **1997**, *66*, 385–407.

[2] C. L. Masters, G. Simms, N. A. Weinman, G. Multhaup, B. L. McDonald, K. Beyreuther, *Proc. Natl. Acad. Sci.* **1985**, *82*, 4245–4249.

[3] K. Beyreuther, C. L. Masters, *Brain Pathol.* **1991**, *1*, 241–251.

[4] E. Cohen, J. Bieschke, R. M. Perciavalle, J. W. Kelly, A. Dillin, *Science* **2006**, *313*, 1604–1610.

[5] C. Haass, D. J. Selkoe, *Nat. Rev. Mol. Cell Biol.* **2007**, *8*, 101–12.

[6] E. Betzig, G. H. Patterson, R. Sougrat, O. W. Lindwasser, S. Olenych, J. S. Bonifacino, M. W. Davidson, J. Lippincott-Schwartz, H. F. Hess, *Science* **2006**, *313*, 1642–1645.

[7] S. T. Hess, T. P. K. Girirajan, M. D. Mason, *Biophys. J.* **2006**, *91*, 4258–72.

[8] M. J. Rust, M. Bates, X. W. Zhuang, *Nat Methods* **2006**, *3*, 793–795.

[9] M. Heilemann, S. van de Linde, M. Schüttpelz, R. Kasper, B. Seefeldt, A. Mukherjee, P. Tinnefeld, M. Sauer, *Angew. Chemie Int. Ed.* **2008**, *47*, 6172–6176.

[10] T. Ha, P. Tinnefeld, *Annu. Rev. Phys. Chem.* **2012**, *63*, 595–617.

[11] B. Kozankiewicz, M. Orrit, *Chem. Soc. Rev.* **2014**, *43*, 1029–1043.

[12] A. Sharonov, R. M. Hochstrasser, *Proc. Natl. Acad. Sci.* **2006**, *103*, 18911–18916.

[13] D. Sage, H. Kirshner, T. Pengo, N. Stuurman, J. Min, S. Manley, M. Unser, *Nat. Methods* **2015**, *12*, 717–724.

[14] E. Betzig, *Angew. Chemie Int. Ed.* **2015**, *54*, 8034–8053.

[15] S. W. Hell, *Angew. Chemie Int. Ed.* **2015**, *54*, 8054–8066.

[16] W. E. Moerner, *Angew. Chemie Int. Ed.* **2015**, *54*, 8067–8093.

[17] C. Eggeling, M. Heilemann, *Curr. Opin. Chem. Biol.* **2014**, *20*, v–vii.

[18] G. S. Kaminski Schierle, S. van de Linde, M. Erdelyi, E. K. Es er, T. Klein, E. Rees, C. W. Bertoncini, C. M. Dobson, M. Sauer, C. F. Kaminski, *J. Am. Chem. Soc.* **2011**, *133*, 12902–12905.

[19] D. Pinotsi, G. S. Kaminski Schierle, C. F. Kaminski, in *Syst. Biol. Alzheimer's Dis.*, Humana Press, New York, NY, **2016**, pp. 125–141.

[20] H. A. Shaban, C. A. Valades-Cruz, J. Savatier, S. Brasselet, *Sci. Rep.* **2017**, *7*, 1–10.

[21] H. Shroff, C. G. Galbraith, J. A. Galbraith, E. Betzig, *Nat. Methods* **2008**, *5*, 417–423.

[22] R. P. J. Nieuwenhuizen, K. a Lidke, M. Bates, D. L. Puig, D. Grünwald, S. Stallinga, B. Rieger, *Nat. Methods* **2013**, *10*, 557–562.

[23] J. Ries, V. Udayar, A. Soragni, S. Hornemann, K. P. R. Nilsson, R. Riek, C. Hock, H. Ewers, A. A. Aguzzi, L. Rajendran, *ACS Chem. Neurosci.* **2013**, *4*, 1057–1061.

[24] R. Jungmann, M. S. Avendaño, J. B. Woehrstein, M. Dai, W. M. Shih, P. Yin, *Nat. Methods* **2014**, *11*, 313–318.

[25] J. Molle, M. Raab, S. Holzmeister, D. Schmitt-Monreal, D. Grohmann, Z. He, P. Tinnefeld, *Curr. Opin. Biotechnol.* **2016**, *39*, 8–16.

[26] M. Biancalana, S. Koide, *Biochim. Biophys. Acta - Proteins Proteomics* **2010**, *1804*, 1405–1412.

[27] H. LeVine, in *Methods Enzymol.*, Elsevier Inc., **1999**, pp. 274–284.

[28] H. Bennhold, *Münchener Medizinische Wochenschriften* **1922**, 1537.

[29] T. Ban, D. Hamada, K. Hasegawa, H. Naiki, Y. Goto, *J. Biol. Chem.* **2003**, *278*, 16462–16465.

[30] A. I. Sulatskaya, I. M. Kuznetsova, M. V. Belousov, S. A. Bondarev, G. A. Zhouravleva, K. K. Turoverov, *PLoS One* **2016**, *11*, e0156314.

[31] M. Ovesný, P. Křížek, J. Borkovec, Z. Švindrych, G. M. Hagen, *Bioinformatics* **2014**, *30*, 2389–2390.

[32] A. E. Roher, M. O. Chaney, Y. Kuo, S. D. Webster, W. B. Stine, L. J. Haverkamp, A. S. Woods, R. J. Cotter, J. M. Tuohy, G. a Krafft, et al., *J. Biol. Chem.* **1996**, *271*, 20631–20635.

[33] B. Rieger, S. Stallinga, *ChemPhysChem* **2014**, *15*, 664–670.

[34] Y. Hu, T. Guo, X. Ye, Q. Li, M. Guo, H. Liu, Z. Wu, *Chem. Eng. J.* **2013**, *228*, 392–397.

[35] C. Wu, M. Biancalana, S. Koide, J.-E. Shea, *J. Mol. Biol.* **2009**, *394*, 627–633.

[36] J. Bieschke, J. Russ, R. P. Friedrich, D. E. Ehrnhoefer, H. Wobst, K. Neugebauer, E. E. Wanker, *Proc. Natl. Acad. Sci.* **2010**, *107*, 7710–7715.

[37] C. E. Aitken, R. A. Marshall, J. D. Puglisi, *Biophys. J.* **2008**, *94*, 1826–1835.

[38] A. J. Baldwin, T. P. J. Knowles, G. G. Tartaglia, A. W. Fitzpatrick, G. L. Devlin, S. L. Shammas, C. A. Waudby, M. F. Mossuto, S. Meehan, S. L. Gras, et al., *J. Am. Chem. Soc.* **2011**, *133*, 14160–14163.

Entry for the Table of Contents

FULL PAPER

Transient amyloid binding (TAB) imaging resolves amyloid structures at a nanometer scale using standard probes, Thioflavin T (ThT), without the need for covalent modification or immunostaining of amyloids. Binding dynamics and blinking of ThT molecules on amyloids enables continuous imaging over extended times without image degradation due to photobleaching, and gives robust imaging to various amyloid structures and imaging conditions.

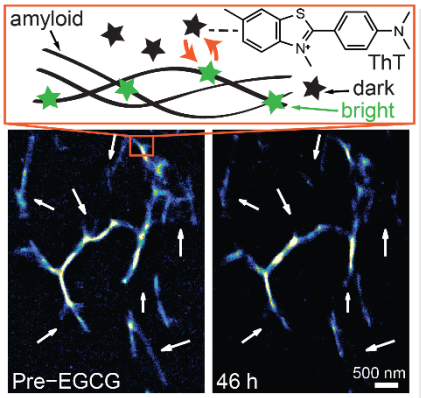

Kevin Spehar+, Tianben Ding+, Yuanzi Sun, Niraja Kedia, Jin Lu, George R. Nahass, Matthew D. Lew, Jan Bieschke**

Page No. – Page No.

Super-Resolution Imaging of Amyloid Structures over Extended Times Using Transient Binding of Single Thioflavin T Molecules

Supporting Information

Super-Resolution Imaging of Amyloid Structures over Extended Times Using Transient Binding of Single Thioflavin T Molecules

Kevin Spehar[+], Tianben Ding[+], Yuanzi Sun, Niraja Kedia, Jin Lu, George R. Nahass, Matthew D. Lew*, Jan Bieschke*

Abstract: Oligomeric amyloid structures are crucial therapeutic targets in Alzheimer's and other amyloid diseases. However, these oligomers are too small to be resolved by standard light microscopy. We have developed a simple and versatile tool to image amyloid structures using Thioflavin T without the need for covalent labeling or immunostaining. Dynamic binding of single dye molecules generates photon bursts that are used for fluorophore localization on a nanometer scale. Thus, photobleaching cannot degrade image quality, allowing for extended observation times. Super-resolution Transient Amyloid Binding (TAB) microscopy promises to directly image native amyloid using standard probes and record amyloid dynamics over minutes to days. We imaged amyloid fibrils from multiple polypeptides, oligomeric, and fibrillar structures formed during different stages of amyloid-β aggregation, as well as the structural remodeling of amyloid-β fibrils by the compound epi-gallocatechin gallate (EGCG).

DOI: 10.1002/anie.2016XXXXX

Table of Contents

Supporting Notes

Unless stated otherwise, all chemicals were purchased from Sigma-Aldrich and are ACS grade.

1. Aβ42 and Aβ40 Preparation

Crude Aβ42 and Aβ40 peptide purchased from Watsonbio Sciences was purified *via* reverse-phase high-performance liquid chromatography (HPLC), lyophilized, then dissolved in hexafluoro-2-propanol (HFIP), and sonicated at room temperature for one hour in a water bath sonicator. After freezing in liquid nitrogen, HFIP was removed by lyophilization, and aliquots of the peptide were stored at −20 °C. To prepare unlabeled monomer, lyophilized Aβ42 and Aβ40 were dissolved in 10 mM NaOH, sonicated for 25 min in a cold water bath, and filtered first through a 0.2 μm and then through a 30 kD membrane filter (Millipore) as described previously.[1]

To prepare fibrils, we incubated 10 μM monomeric Aβ40 in PBS (150 mM NaCl, 50 mM Na_3PO_4, pH 7.4) at 37 °C with 5 seconds of shaking every 10 minutes in a non-binding 96-well black wall, clear bottom (Corning 3651) plate. 20 μM ThT was added for monitoring fibril aggregation kinetics using the ThT fluorescence in a microplate reader (Tecan, Infinite F200). Samples were removed and flash frozen in liquid nitrogen at various time points to obtain samples from different stages of Aβ40 aggregation (8 hours, 24 hours, 66 hours). Monomeric Aβ42 (60 - 110 μM) was aggregated at 37 °C in PBS with shaking for 24 hours under analogous conditions.

2. Imaging Sample Preparation

8-well cell culture chambers with optical glass coverslip bottom (Lab Tek, No. 1.5H, 170 ± 5 μm thickness) were cleaned using a UV Ozone Cleaner (Novascan Technologies) for 15 minutes. Amyloid solutions were prepared as described in “Aβ42 and Aβ40 Preparation”. 10 μL solution + 20 μL distilled water (dH_2O) was adsorbed to the coverslip for 1 hour. The coverslip was rinsed with 500 μL dH_2O. To prevent unspecific binding of ThT to the glass surface, 2% (w/v) Bovine Serum Albumin (BSA) (200 μL in dH_2O) was incubated on the coverslip for 10 minutes and then rinsed off using 500 μL dH_2O.

3. Aβ42 Monomer Labeling Procedure

HPLC-purified synthetic Aβ42 that carried an N-terminal cysteine (Watson bio) was dissolved in 10 mM NH_4OH and sonicated on ice for 30 minutes. The dissolved Aβ42 was mixed in equal volume with a solution of 50 mM NH_4HCO_3 and 50 μM tris(2-carboxyethyl)phosphine (TCEP) with pH of 4. This final solution had pH between 7.0 and 7.5. The solution was transferred to a glass vial with stir bar. Alexa-647 C_2 Maleimide (ThermoFisher Scientific, A20347) in DMSO solution (30 μL of 10 mg/mL) was added to the solution while stirring. The solution was stirred overnight at 5 °C in the dark. Afterwards, 2 μL of β-mercaptoethanol (BME) was added to the solution. The solution was then frozen in liquid nitrogen and lyophilized. The lyophilized peptide was dissolved in 1 mL formic acid, and the solution was diluted 1:1 with dH_2O before purified by high performance liquid chromatography (HPLC). The solution was then frozen in liquid nitrogen and lyophilized. Finally, the peptide was dissolved in hexafluoro-2-propanol (HFIP), and frozen in liquid nitrogen and lyophilized.

4. Intrinsically-Labeled Aβ42 Preparation

80 μg of unlabeled monomeric Aβ42 in 100 μL of 10 mM NaOH and 0.8 nmol of monomeric Aβ42 covalently labeled with Alexa Fluor 647 C_2 Maleimide in 20 μL of 10 mM NaOH were mixed and sonicated on ice for 25 min. The mixture was filtered by centrifugation through a 0.2 μm and then through a 30 kD membrane filter. Peptide concentration and fraction of labeled monomer (4.2%) were calculated from UV-Vis absorption spectra (Implen, Nanophotometer, P330). Monomeric Aβ42 peptide (50 μM) was incubated at 37 °C for 40 hours without shaking. The fibrils were adsorbed to the coverslip as described in “Imaging Sample Preparation”.

5. Antibody-Labeled Aβ42 Preparation

2% BSA in 200 μL of PBS with mouse anti-Aβ antibody 6E10 (Signet 9320) primary antibody (1:300 dilution) was incubated on the coverslip prepared in “Imaging Sample Preparation” for 1.5 hour. Afterwards, the coverslip was washed with 200 μL PBS for 5 times. Then 2% BSA in 200 μL of PBS with Alexa-647 labeled Goat Anti-Mouse IgG secondary antibody (1:200 dilution, Thermo Fisher Scientific, A-21236) was added to the coverslip and left for 1 hour. Afterwards, the coverslip was washed with 200 μL PBS 5 times.

6. α-Synuclein Preparation

α-synuclein was expressed in *Escherichia coli* and purified as described previously[2] and then lyophilized for storage. Lyophilized protein was dissolved in 10 mM NaOH to final concentration of 1 mg/mL, vortexed gently and sonicated in a water bath at 20 °C for 15 minutes. The suspension was then centrifuged at 50,000 RPM at 4 °C for 20 minutes after which the supernatant was collected. 90 μM α-synuclein was aggregated in 40 μM ThT and 200 mM Na_3PO_4 with a 2 mm glass bead. Aggregation kinetics were recorded on an InfinitE M200 Tecan plate reader with a shake time of 5 seconds, kinetic interval of 15 minutes, amplitude of 1 mm for 400 cycles. The sample was adsorbed onto a glass coverslip as described in “Imaging Sample Preparation”.

7. IAPP Preparation

HPLC purified 37 aa islet amyloid polypeptide (IAPP) purchased from R. Volkmer (Charite, Berlin) was dissolved in hexafluoro-2-propanol (HFIP) and sonicated at room temperature for one hour in a water bath sonicator. After freezing in liquid nitrogen, HFIP was removed by lyophilization, and aliquots of the peptide were stored at −20 °C. To prepare unlabeled monomer, lyophilized IAPP was dissolved in 10 mM NaOH, sonicated for 25 min in cold water bath, and filtered first through a 0.2 μm and then through a 30 kD

membrane filter (Millipore). IAPP fibrils were formed by incubating 30 μM monomeric peptide in 150 mM NaCl, 50 mM Na_3PO_4, pH 7.4 with 20 μM ThT at 37 °C with 5 seconds of shaking every 10 minutes. Fibril formation was monitored by measuring aggregation kinetics through ThT fluorescence in a microplate reader (Tecan, InfinitE F200). Samples were taken out after 24 hours and adsorbed onto a glass coverslip as described in "Imaging Sample Preparation".

8. Tau Protein Preparation

The wild type 2N4R tau protein (TauRD) was a generous gift from Marc Diamond (UT Southwestern). The protein was expressed and purified as previously described.[3,4] Tau RD was lyophilized in tubes. To dissolve the protein, 20 μL of 100 mM dithiothreitol (DTT), 50 μL of 400 mM NaCl, 50 μL of 40 mM HEPES (4-(2-hydroxyethyl)-1-piperazineethanesulfonic acid), and 48 μL of dH_2O was added to the tube in this order. This was incubated at 20 °C for 1 hour. Afterwards, 32 μL of 50 μM heparin was added. This was then incubated at 20 °C for 17 hours, allowing it to fibrilize. The sample was then adsorbed onto a glass coverslip as described in "Imaging Sample Preparation".

9. Light Chain Preparation

Immunoglobulin light chain (λ-AL-1) was purified from urine of patients suffering from light chain amyloidosis as previously published.[5] The diagnosis of AL Amyloidosis was established via Congo red staining of fat aspirates and/or tissue biopsies[6] at the Amyloidosis Center Heidelberg according to established clinical protocols and in compliance with the ethical guidelines for treatment and patient consent. To form amyloid fibrils, AL protein (40 μM) was incubated in glycine buffer pH 2.8, 150 mM NaCl, 8 mM DTT, 0.05% sodium azide for 7 days under permanent shaking with 200 rpm at 37 °C in a non-binding 1.5 mL tube. The sample was adsorbed onto a glass coverslip as described in "Imaging Sample Preparation" for imaging.

10. Optical Instrumentation

Two epi-fluorescence microscopes were used for TAB imaging (Fig. 1A, Fig. S1, and Table S1).

Microscope 1: This home-built system captures fluorescence using two polarization channels.[7] Samples were illuminated with an inclined 488 nm or 637 nm excitation laser (Coherent, OBIS 488 LX150, OBIS 637 LX140, 30° tilt from normal illumination) through an oil-immersion objective lens (Olympus, UPLSAPO100XO/1.4 NA oil). Fluorescence was collected by the same objective and filtered by appropriate dichroic and bandpass filters. Afterward, the fluorescence was passed through a polarizing beam splitter (Meadowlark optics, BB-100-VIS), and the two separated orthogonally-polarized channels were captured by a scientific CMOS camera (Hamamatsu, C11440-22CU). Although this system can modulate phase in the Fourier plane and create polarized fluorescence images, these capabilities were not utilized in this work.

Microscope 2: This commercial microscope (Nikon, Eclipse Ti Microscope) utilizes a 100X objective (Nikon, ApoTIRF 100X/1.49 NA oil) into which a 488 nm excitation laser (Coherent, Sapphire 488 LP-150) was coupled for high incident angle illumination (75° tilt from normal illumination). Fluorescence signals were collected through a custom filter cube, and captured by an electron-multiplying CCD camera (Andor, iXon 897).

11. Imaging Procedure

Images of TAB and intrinsically/antibody-labeled Aβ42 were captured as follows. Tables S2 and S3 list the detailed buffers and conditions under which each image was acquired.

TAB Imaging: 200 μL of an imaging buffer containing ThT, NaCl, and Na_3PO_4 was placed into the amyloid adsorbed chambers. Super-resolution imaging was performed using a 488 nm excitation laser. The peak intensities of the lasers at the sample were 2.2 kW/cm^2 in microscope 1 and 0.51 kW/cm^2 in microscope 2. Stacks of 5,000 or 10,000 images of 20 ms exposure were recorded.

Intrinsically/Antibody-Labeled Aβ42 Imaging: An enzymatic oxygen-scavenging buffer containing glucose, glucose oxidase, catalase, and thiol (Buffer 2, Table S2) was used to image the intrinsically-labeled and antibody-labeled Aβ42 samples. Due to a non-uniform and sparse labeling density, only a standard diffraction-limited image could be produced from the Alexa-647 dye with 637 nm excitation in microscope 1. Afterwards, the illumination was switched to the 488 nm laser, and TAB imaging was performed on the same fibril in the presence of 1 μM ThT. Super-resolution imaging was performed on the Alexa-647 labeled antibody using the 637 nm excitation laser (peak intensity: 10 kW/cm^2) in microscope 1. A TAB image was taken of the Alexa-647 labeled fibril using 488 nm excitation in a similar manner as TAB imaging of intrinsically-labeled Aβ42. Image stacks of 10,000 frames with 15 ms exposure were captured for Alexa-647 dSTORM.

Time-lapse imaging of amyloid remodeling: Aβ42 fibrils were adsorbed to ozone-cleaned chambers as described in "Imaging Sample Preparation", but this time without the BSA incubation for increasing reachability of EGCG to amyloid structures. EGCG (Taiyo International, Sunphenon EGCg) was added to an imaging buffer in the amyloid adsorbed chambers in order to remodel and dissolve structures of amyloid fibrils.[8] After variable-length incubations (as indicated in Figs. 4 and S7, and Supporting Movie S1) in the presence of 1 mM EGCG at room temperature (21 °C), the sample was rinsed and replaced with the ThT imaging buffer for TAB imaging. This procedure was repeated over 46 hours.

12. Atomic Force Microscopy

Aliquots of Aβ aggregation time points (10 μl) were placed on a clean, freshly cleaved grade V-1 mica (Cat#: 01792-AB, Structure Probe, Inc., USA). After 10 minutes, the solvent was wicked off by filter paper and the mica was washed 4 times with 20 μl of water to remove salts and buffer from the sample. Samples were dried overnight, and AFM images were acquired in tapping mode on a Veeco Dimension 3100 machine (Bruker) with Bruker FESP tips.

13. Quantification of Photons Detected, Background Photons, and Localization Precision

The captured image stacks were offset corrected by subtracting dark images. Images were then localized using the ThunderSTORM plugin[9] within ImageJ using default settings except the following: camera parameters were set as in Table S1; a peak intensity threshold was set between std(Wave.F1) and 2.5*std(Wave.F1) to avoid false localizations of background fluorescence. Post-processing on the images captured in microscope 1 and 2 was performed using custom analysis scripts written in MATLAB (Mathworks, R2016a, R2017a). A list of estimated single-molecule positions (x, y) and point spread function (PSF) widths (σ) was produced by ThunderSTORM. Detected photons per localization were obtained by summing all photons within a region of interest (7×7 pixels in microscope 1, 3×3 pixels in microscope 2) centered at the location (x, y) of each molecule. This integrated photon count was then background corrected using the average photons per pixel in the surrounding region (Fig. S2A). The following filtering was performed to reject false localizations due to background fluorescence and low signal-to-noise ratio: localizations of single-molecules were only retained if: 1) the number of photons detected was larger than 100, and 2) the measured PSF widths were reasonable (50 nm $< \sigma <$ 150 nm in microscope 1, 100 nm $< \sigma <$ 260 nm in microscope 2). The estimated localization precision, or the best possible localization uncertainty for the least-squares fitting algorithm, was calculated based on the photons detected and the background as previously described.[10]

14. Dual-Channel Registration

A registration process was required for analyzing dual-channel images captured in microscope 1. The geometric transformation between the two channels on the sCMOS camera was calibrated using fluorescent beads (Thermo Fisher Scientific, FluoSpheres, 0.1 μm, 505/515, F8803) adsorbed onto an ozone-cleaned 8-well cell culture chamber. Image acquisition of these beads was performed immediately after single-molecule super-resolution imaging. 4,000 - 180,000 photons per bead were detected with 20 ms exposure time. We imaged each bead over 8 - 10 frames, and calculated the bead positions by averaging the localizations across multiple frames from ThunderSTORM. All possible lines joining pairs of bead positions across the two channels were drawn. Control points for two-channel registration were selected by comparing the obtained lines, and keeping the largest ensemble of them with similar lengths and slopes. To create the two-channel registration map, coefficients of a global 2D polynomial transformation function were calculated using the control points as input to the *fitgeotrans* function included with MATLAB. Although the performance of the dual-channel registration map was improved by immediate calibration after single-molecule imaging, there was still a small amount of registration error when we applied the calibrated transformation function on localized single-molecule positions. This small and spatially-varying bias was most likely due to system drift between measurements. We refined the registration map by re-calculating the global 2D polynomial transformation using the scheme described above, but this time using the single-molecule localizations with high localization precision (< 20 nm). Finally, localized single molecules were paired across the two channels by selecting the nearest neighbor in the target channel to the transformed position from the source channel, within a spatial range corresponding to 3 times the localization precision. The average of the positions from the transformed and target channels is taken to be the location of the paired single molecule. All paired and unpaired localized positions were kept for reconstructing super-resolved images of amyloid structures and measuring photons detected and localization precision. For paired localizations, the sum across the two channels was designated as the number of photons detected (Fig. S2D) and background (Fig. S2E). The calculated localization precisions from both channels were concatenated and reported as the localization performance of TAB imaging in microscope 1 (Fig. S2F).

15. Amyloid Structure Reconstruction and Region of Interest Selection

2D amyloid structures were visualized by assembling and binning all single-molecule localizations within 20×20 nm^2 bins (Fig. S2B). The full-width at half-maximum (FWHM) of cross-section profile was measured over the length of reconstructed fibrils to characterize apparent fibril widths. An additional region of interest (ROI) selection was applied on the reconstructed image in order to extract ThT blinking characteristics on the structures of interest. The super-resolution image was converted into a binary image based on a threshold of 2 localizations/bin. Afterward, the largest connected structure was found from the image using the *bwconncomp* function in MATLAB after filling holes in the binary image using *imfill*. The boundary of the ROI was detected by *bwtraceboundary* in MATLAB, and the photon statistics of the localizations within the boundary were analyzed and reported for characterizing TAB super-resolution images.

16. Localization Grouping across Consecutive Frames

In order to quantify the kinetics of ThT fluorescence measured across multiple camera frames, we grouped localizations of ThT blinking together into “bursts”. Localized ThT molecules in a frame were grouped with localizations in the consecutive frames by selecting the nearest neighbors within a spatial circle corresponding to 3 times the localization precision. Photons detected from the grouped localizations were summed and designated as total photons detected per burst (Fig. S2H). The length (or on-time) of each ThT burst was reported as the number of frames within which localizations were successfully grouped, in units of exposure time (20 ms, Fig. S2I). The time constant of a fit to an exponential decay was obtained to measure the mean of on-time of all ThT bursts.

17. Imaging Buffer Comparison

We varied the NaCl and ThT concentrations, and pH of the imaging buffer to test ThT blinking on amyloid structures under different imaging conditions. For the NaCl comparison, 4 different NaCl concentrations (10, 150, 300, 500 mM) were tested with 20 mM Na_3PO_4, 1 μM ThT, pH 8.6. We imaged 12 unique Aβ42 fibrils for each condition. Photons detected per localization, background photons per pixel, photons detected per burst, on-time per burst, and localization rate were reported (Fig. S3A). ThT blinking under 5 different pH (6.0, 6.8, 7.4, 8.0, 8.6) was quantified with 500 mM NaCl and 1 μM ThT. For this measurement, we imaged 5 identical Aβ42 fibrils using the different buffers. Similarly, ThT concentration (0.1, 0.5, 1, 2, 5 μM) influence on TAB performance was tested using 3 long identical Aβ42 fibrils with 150 mM NaCl and pH 7.4. The imaging buffers were exchanged completely between each imaging acquisition in a random order. Analogous ThT statistics were reported in Fig. S3B.

Supporting Figures

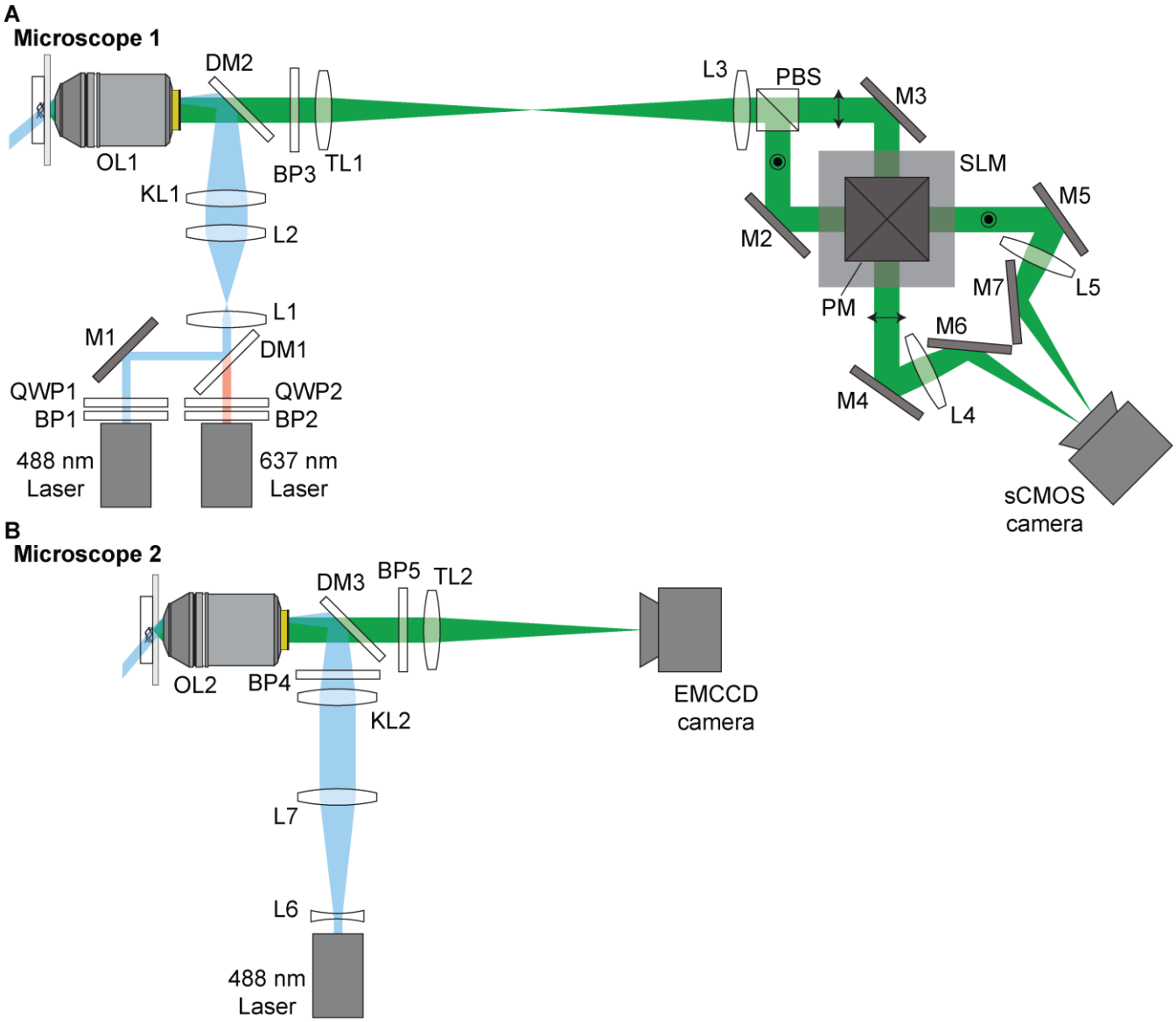

Figure S1. Detailed schematics of the optical setups. (A) Microscope 1. Circularly-polarized 488 nm and 637 nm lasers were used for illumination during TAB and intrinsically/antibody-labeled imaging, respectively. After beam expansion by lenses L1 (f = 25.4 mm) and L2 (f = 76.2 mm), the excitation lasers were coupled into a 100X oil-immersion objective (OL1, 1.4 NA) for highly-inclined illumination. Fluorescence was collected by the same objective and filtered by dichroic (DM2) and bandpass (BP3) filters listed in Table S1. Afterward, the fluorescence was split by a polarizing beam splitter (PBS) into two orthogonally-polarized channels, and lens L3 (f = 150 mm) projects the pupil plane onto a spatial light modulator (SLM) using a square pyramidal mirror (PM). After reflection, the two channels were imaged onto different portions of the sCMOS camera by lenses L4 and L5 (f = 150 mm). Although this system can modulate the phase of fluorescence in the Fourier plane using the SLM,[7] this capability was not utilized in this work. (B) Microscope 2. Pseudo-TIRF illumination excites fluorophores within the sample. Collected fluorescence was filtered by a custom filter cube containing a dichroic mirror (DM3) and a bandpass filter (BP4) before being captured by an EMCCD camera.BP1-5, bandpass filters; QWP1-2, quarter wave plates; M1-7, mirrors; DM1-3, dichroic mirrors; L1-7, lenses; KL1-2, widefield lenses; OL1-2, objective lenses; TL1-2, tube lenses.

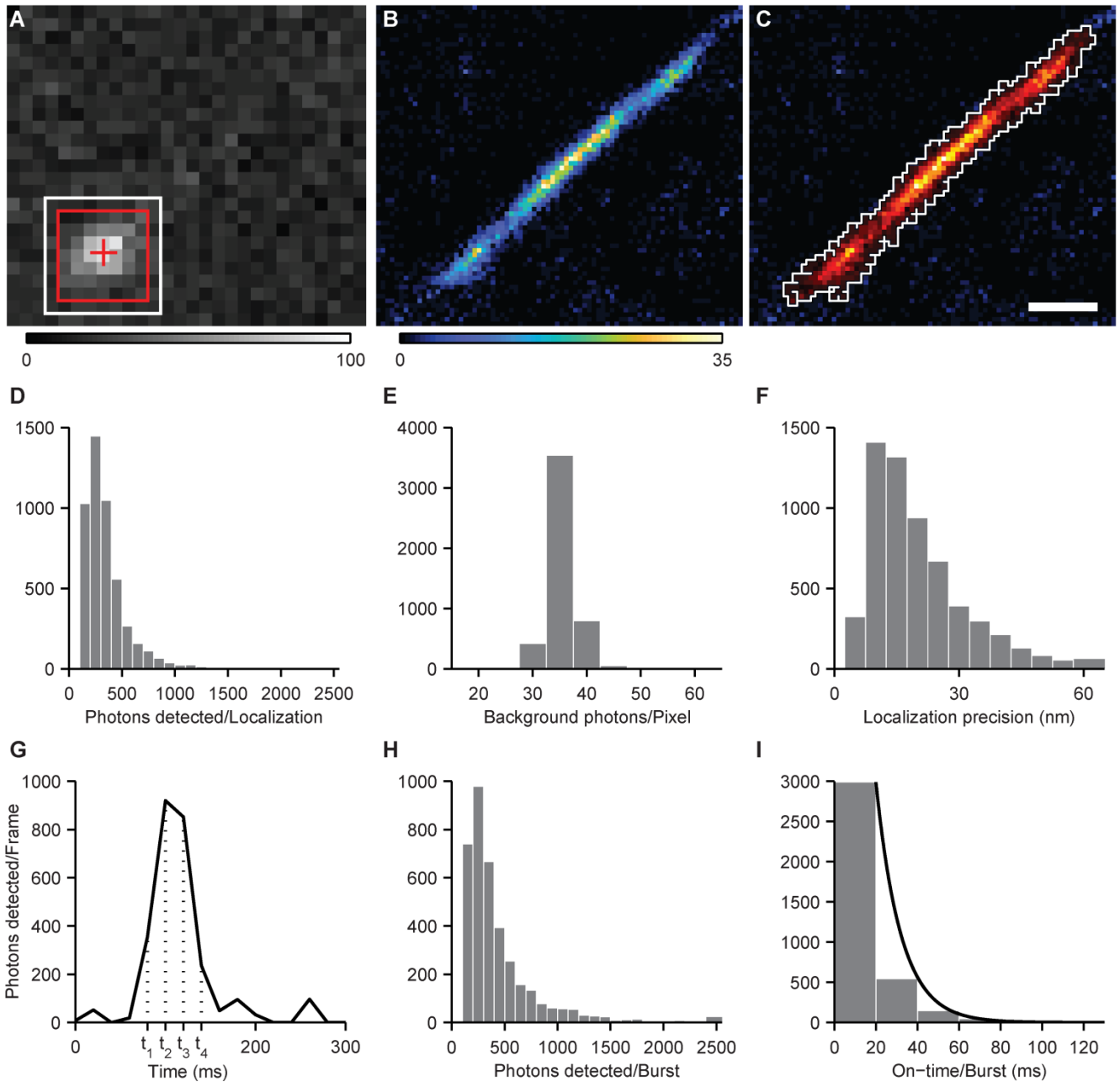

Figure S2. Analysis of ThT localization and blinking events. (A) A captured ThT blinking event on an Aβ42 fibril in microscope 1. Gray scale denotes the number of photons detected per pixel. Detected photons per localization were calculated by integrating all photons within a region of interest (red square) centered at the location output by ThunderSTORM (red cross). The integrated photon number was then background corrected using the average photons within the surrounding pixels between the red and white squares. (B) TAB super-resolution image of the Aβ42 fibril after the filtering and the two channel registration process described in Supporting Notes 13 and 14. The color scale denotes the number of localizations per bin. (C) Region of interest (ROI) selection (Supporting Note 15). The hot color scale shows the region of interest associated with the fibril, while the white line depicts the boundary of this ROI. Scale bar: 300 nm. (D-F) Histograms of photons detected/localization, background photons/pixel, and the localization precision of ThT bursts observed in the image stack (5000 frames, 100 s) within the ROI. (G) Photons detected over time in the red square in A. Localizations over consecutive frames (t1-t4) were grouped together as a single "burst", and the detected photons from each ThT burst were analyzed after the localization grouping process (Supporting Note 16). (H and I) Histograms of photons detected and the on-time of ThT bursts after the localization grouping process. Black solid line in I depicts the fitting result to an exponential decay. The median of photons detected per burst was 319; the time constant of the exponential fit was 12 ms. This data corresponds to the fibril shown in Fig. 1D in the main text.

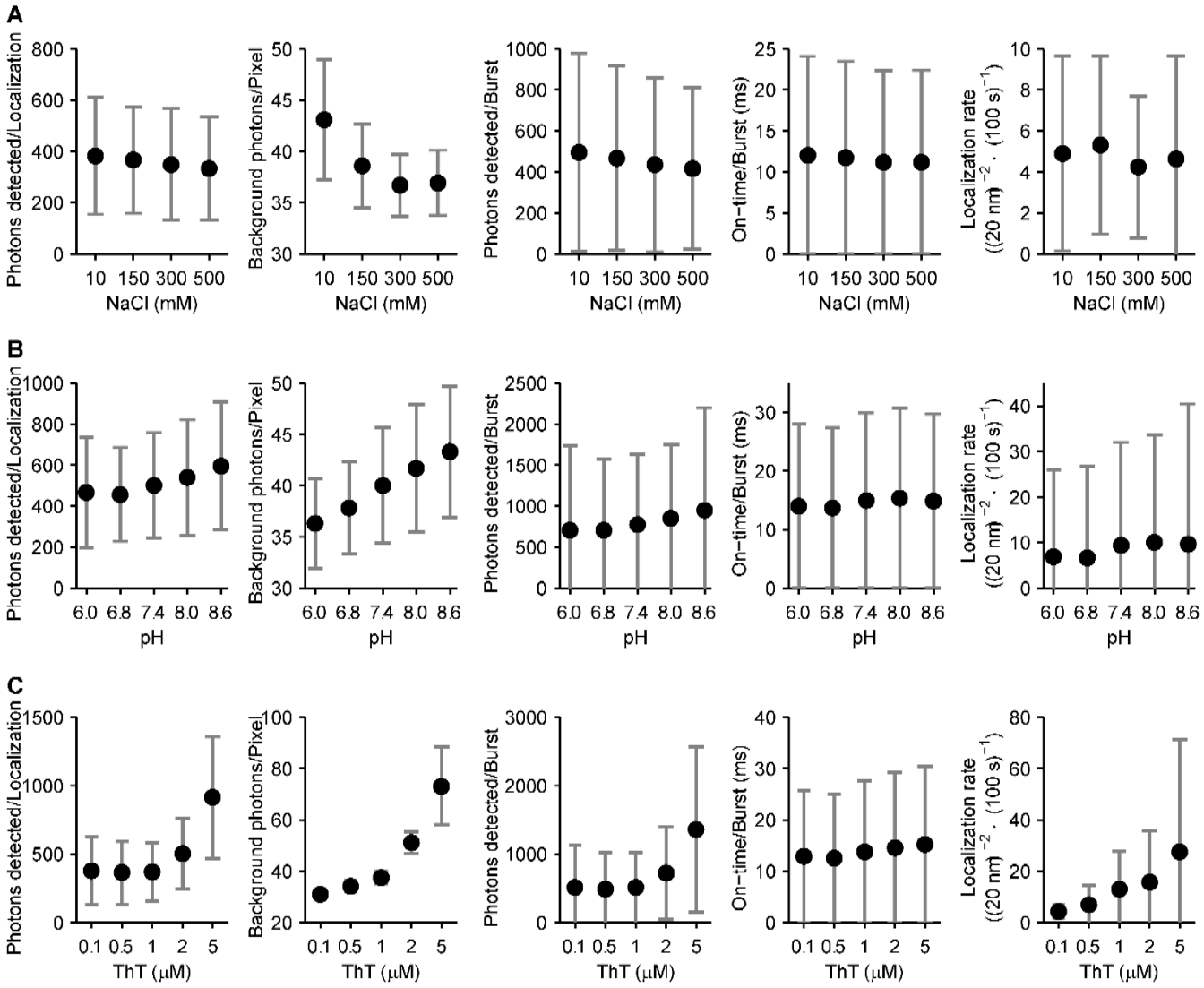

Figure S3. Imaging buffer effects on ThT blinking. ThT blinking characteristics were measured under varying (A) NaCl concentration (10 – 500 mM), (B) pH (6.0 – 8.6), and (C) ThT concentration (0.1 – 5 μM). NaCl concentration and pH appear to have limited effect on the blinking of ThT on fibrils. However, reduced background photons/pixel were observed under high NaCl concentration and low pH conditions. On the other hand, the blinking rate of ThT, and thus the rate of locations per time, and background photons rise with increasing ThT concentration. The high blinking rate at 5 μM ThT causes images of overlapping molecules, which leads the number of photons detected and background photons per localization to rise significantly. Dots represent the mean across experiments, error bars represent standard deviations. Negative error bars are truncated at zero.

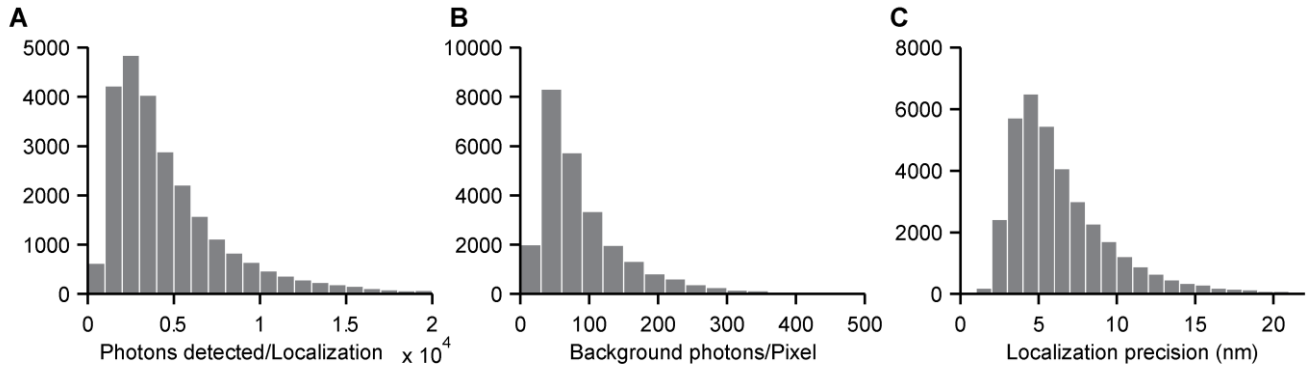

Figure S4. Analysis of Alexa-647 dSTORM. (A-C) Histograms of photons detected/localization, background photons/pixel, and localization precision of Alexa-647 bursts observed in the image stack (10,000 frames, 150 s).

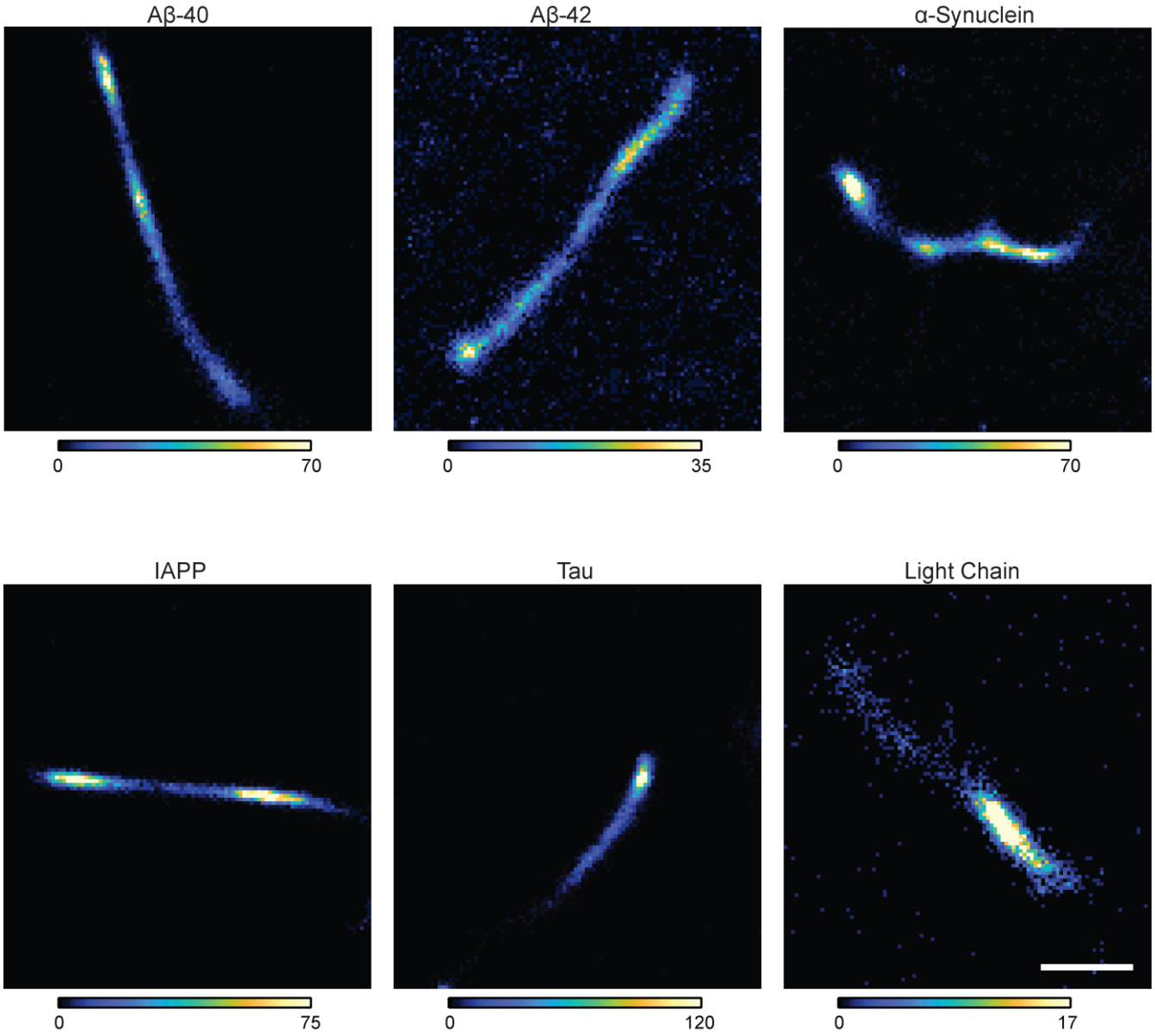

Figure S5. TAB super-resolution images of Aβ40, Aβ42, α-Synuclein, IAPP, Tau, and Light Chain. Scale bar: 500 nm. Color bars in units of localizations/bin.

Figure S6. The localization rate of single ThT molecules during TAB imaging. (A) Localizations per 100 frames over time during the acquisition of imaging stacks for each TAB image in the main text. Localizations over time were approximately constant over time with no evidence of photobleaching. The discontinuity in

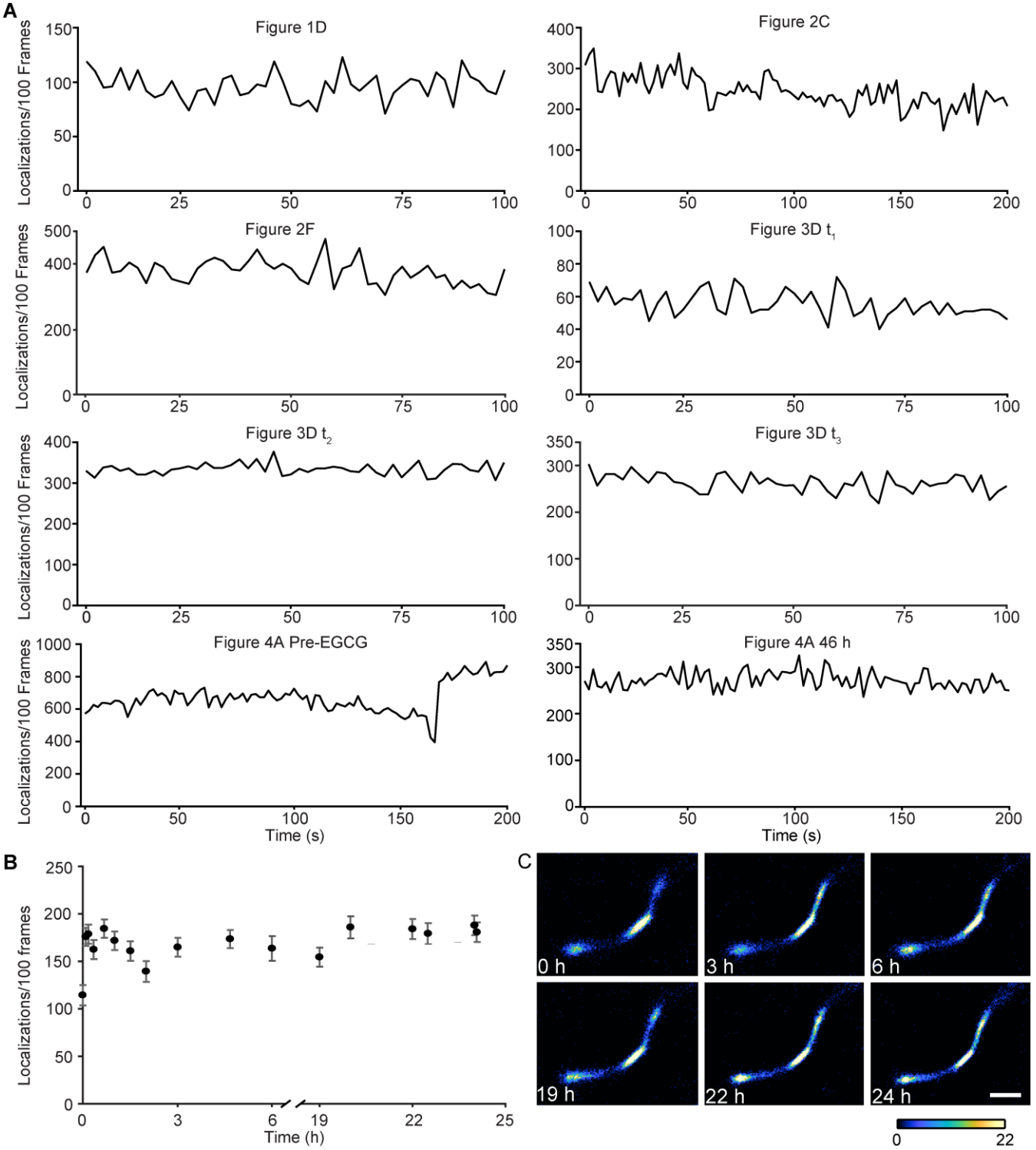

Figure 4A Pre-EGCG was due to refocusing the microscope at ~320 s into the measurement. (B) The localization rate of ThT molecules for multiple TAB images over an extended observation time. 17 time-lapse TAB image stacks were taken on an Aβ42 fibril over 24 h without changing ThT imaging buffer. The stable localization numbers show that long-term TAB imaging is feasible. (C) TAB image reconstructions at select time points from the plot in B. Images show consistent reconstruction quality of the same fibril over 24 hours. Scale bar: 500 nm. Color bar in units of localizations/bin.

Figure S7. Time-lapse TAB super-resolution images of Aβ42 before and 7, 22, 29, 46, 50 h after adding EGCG. The fibril was incubated with 1 mM EGCG at room temperature as described in Supporting Note 11 except for the final incubation during 46-50 h. More concentrated EGCG was added to make an 8 mM

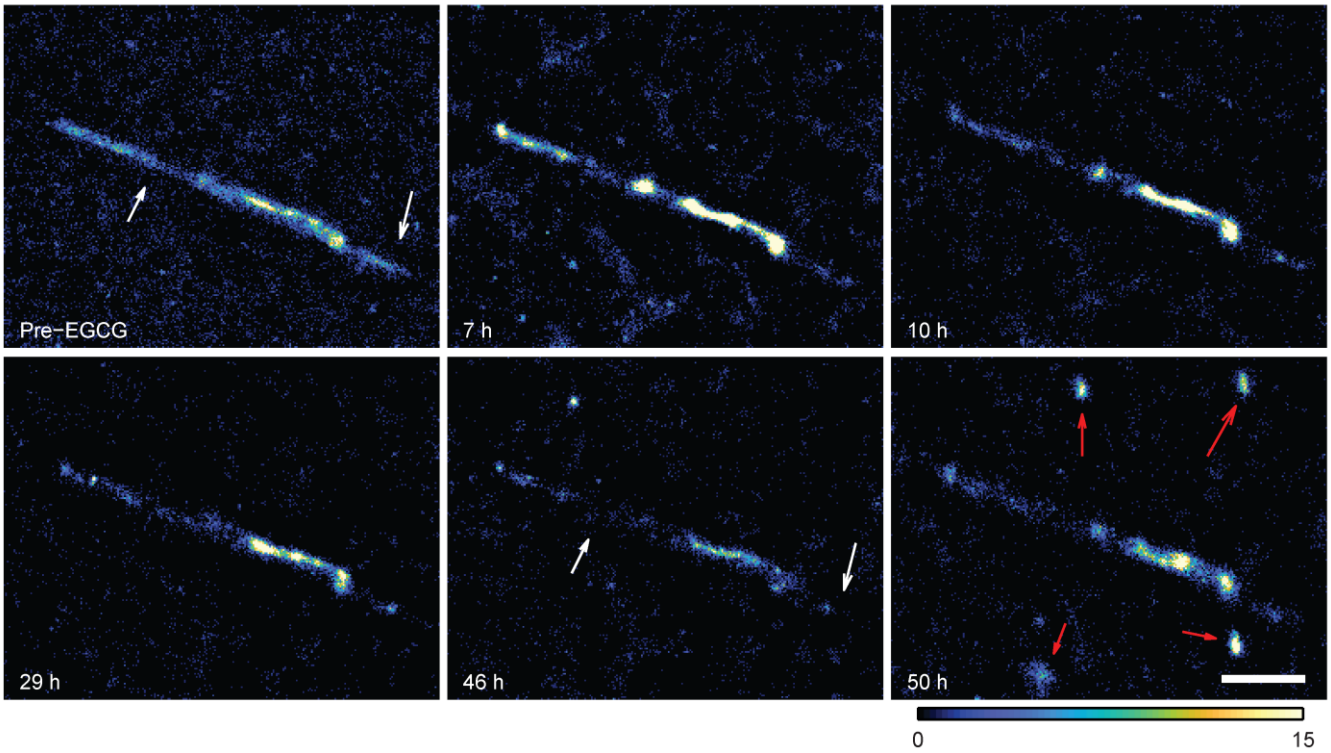

EGCG buffer during this period in order to accelerate fibril remodeling. Gradual fibril dissolution was observed in the first 46 h incubation with 1 mM EGCG (white arrows), and some spherical assemblies were observed after the 4 h incubation in the presence of 8 mM EGCG (red arrows). Similar spherical structures were observed in our previous work using AFM.[8] Scale bar: 1 μm; color bar in units of localizations/bin.

Supporting Tables

Table S1. Components of the optical setups

	Microscope 1	Microscope 2
Basics		
Microscope body	Custom	Nikon Eclipse Ti Microscope
Objective lens	Olympus, UPLSAPO100XO/1.4 NA oil (OL1)	Nikon, ApoTIRF 100X/1.49 NA oil (OL2)
Camera	Hamamatsu, C11440-22CU (sCMOS)	Andor, iXon 897 (EMCCD)
EM Gain	N/A	50
Effective Pixel Size (object space)	58.5 nm	130 nm
TAB imaging		
Excitation Light Source	Coherent, OBIS 488 LX150	Coherent, Sapphire 488 LP-150
Excitation Bandpass Filter	Semrock, FF01-488/6-25 (BP1)	Chroma, ZET488/10x (BP4)
Dichroic Mirror	Semrock, Di03-R488/561-t1 (DM2)	Chroma, ZET488rdc (DM3)
Emission Bandpass Filter	Semrock, FF01-523/610 (BP3)	Chroma, ZET488NF (BP5)
Intrinsically/antibody-labeled imaging		
Excitation Light Source	Coherent, OBIS 637 LX140	N/A
Excitation Bandpass Filter	Semrock, FF01-637/7-25 (BP2)	N/A
Dichroic Mirror	Semrock, Di02-R635 (DM2)	N/A
Emission Bandpass Filter	Semrock, FF01-676/37 (BP3)	N/A

Detailed schematics are shown in Fig. S1. Abbreviations in parentheses refer to corresponding components in Fig. S1.

Table S2. Imaging buffers

	Buffer 1	Buffer 2	Buffer 3	Buffer 4
pH	8.6	8.3	8.3	7.4
NaCl	500 mM	-	-	150 mM
Na_3PO_4	20 mM	-	-	20 mM
ThT	1 μM	-	1 μM	2.5 μM
GLOX + MEA[a]	-	+	+	-

[a] Enzymatic oxygen scavenger (GLOX, glucose oxidase with catalase) and thiol buffer (MEA, β-mercaptoethylamine)[11] consists of two solutions. Solution A: Tris (50 mM, pH 8.3), NaCl (10 mM), glucose (10% w/v), and MEA (Sigma-Aldrich, 30070, 10 mM). Solution B: glucose oxidase (Sigma-Aldrich, G2133, 8 mg), and catalase (Sigma-Aldrich, C100, 38 μL, 21 mg/mL) in PBS (160 μL). The solutions A and B were mixed at the ratio of 99:1 (v/v) immediately before use. + or – refers to the presence or absence of the oxygen scavenger and thiol buffer.

Table S3. Experimental conditions and photon statistics

	Fig. 1BD	Fig. 2A	Fig. 2BC	Fig. 2DE	Fig. 2FG	Fig. 3CD t_1	Fig. 3CD t_2	Fig. 3CD t_3	Fig. 4A
Amyloid	Aβ42	Aβ42	Aβ42	Aβ42	Aβ42	Aβ40	Aβ40	Aβ40	Aβ42
Fluorophore	ThT	Alexa647	ThT	Alexa647	ThT	ThT	ThT	ThT	ThT
Imaging Buffer	1	2	1	2	3	1	1	1	4
Microscope	1	1	1	1	1	2	2	2	1
Photons detected/localization[b]	296	-	425	3718	675	180	381	264	442
Background photons/pixel[b]	35	-	54	71	63	155	195	401	44
Localization precision (nm)[b]	17	-	19	6	15	85	55	111	16

[b] Median of each statistic after the post-processing described in Supporting Notes 13-15.

Supporting Movies

Movie S1. Concatenated time-lapse TAB super-resolution images of Aβ42 before and 3, 7, 10, 22, 25, 29, 34, 46, 50 h after adding EGCG. The reconstructed images correspond to the fibrils shown in Fig. 4 in the main text. The fibrils were incubated at room temperature with 1 mM EGCG for the first 46 h as described in Supporting Note 11 and with 8 mM EGCG for the following 4 h (46-50 h). Log color scale is utilized in order to show structural changes in regions with fewer localizations. In each frame of the movie, TAB SR images from 3 consecutive time points are color-coded using different color maps (colored for current vs grayscale for preceding time points). TAB super-resolution imaging captured the dissolution and remodeling of the fibrils over 50 h. Scale bar: 0.5 µm.

References

[1] N. Kedia, M. Almisry, J. Bieschke, *Phys. Chem. Chem. Phys.* **2017**, *19*, 18036–18046.

[2] H. T. Lam, M. C. Graber, K. A. Gentry, J. Bieschke, *Biochemistry* **2016**, *55*, 675–685.

[3] H. J. Wobst, A. Sharma, M. I. Diamond, E. E. Wanker, J. Bieschke, *FEBS Lett.* **2015**, *589*, 77–83.

[4] B. B. Holmes, S. L. DeVos, N. Kfoury, M. Li, R. Jacks, K. Yanamandra, M. O. Ouidja, F. M. Brodsky, J. Marasa, D. P. Bagchi, et al., *Proc. Natl. Acad. Sci.* **2013**, *110*, E3138–E3147.

[5] K. Andrich, U. Hegenbart, C. Kimmich, N. Kedia, H. R. Bergen, S. Schönland, E. Wanker, J. Bieschke, *J. Biol. Chem.* **2017**, *292*, 2328–2344.

[6] G. Klatskin, *Am. J. Pathol.* **1969**, *56*, 1–13.

[7] M. P. Backlund, M. D. Lew, A. S. Backer, S. J. Sahl, G. Grover, A. Agrawal, R. Piestun, W. E. Moerner, *Proc. Natl. Acad. Sci.* **2012**, *109*, 19087–19092.

[8] J. Bieschke, J. Russ, R. P. Friedrich, D. E. Ehrnhoefer, H. Wobst, K. Neugebauer, E. E. Wanker, *Proc. Natl. Acad. Sci.* **2010**, *107*, 7710–7715.

[9] M. Ovesný, P. Křížek, J. Borkovec, Z. Švindrych, G. M. Hagen, *Bioinformatics* **2014**, *30*, 2389–2390.

[10] B. Rieger, S. Stallinga, *ChemPhysChem* **2014**, *15*, 664–670.

[11] M. Bates, G. T. Dempsey, K. H. Chen, X. Zhuang, *ChemPhysChem* **2012**, *13*, 99–107.

Author Contributions

KS and TD contributed equally to this work. KS, TD, JL, MDL, and JB designed and performed imaging experiments. KS, YS, NK, and GRN prepared amyloid fibrils. TD and MDL built Microscope 1. JB built Microscope 2. TD and KS performed data analysis. KS, TD, MDL, and JB wrote the manuscript.